Dhaka Univ. J. Sci. 59(2): 201-208, 2011 (July)

MHD Heat and Mass Transfer Forced Convection Flow Along a Stretching Sheet with Heat Generation, Radiation and Viscous Dissipation

M. A. Samad[1], Sajid Ahmed[2]and Md. Motaleb Hossain[1]

[1]*Department of Mathematics, Dhaka University, Dhaka-1000, Bangladesh.*

[2]*Institute of Natural Sciences, United International University, Dhaka-1209, Bangladesh*

Received on 15. 04. 2010. Accepted for Publication on 20. 02. 2011

Abstract

The present study comprises of steady two dimensional magnetohydrodynamic heat and mass transfer forced convection flow along a vertical stretching sheet in the presence of magnetic field with radiation and viscous dissipation. The problem has been analyzed by applying Nachtsheim-Swigert shooting iteration technique with sixth order Runge-Kutta integration scheme. The nonlinear partial differential equations governing the flow field occurring in the problem have been transformed to dimensionless nonlinear ordinary differential equations by introducing suitably selected similarity variables. The ensuing equations are simultaneously solved by applying numerical iteration scheme for velocity, temperature and concentration fields. The results are displayed graphically in the form of velocity, temperature and concentration profiles. The corresponding skin-friction coefficient, Nusselt number and Sherwood number are displayed in tabular form. Several important parameters such as the Prandtl number (Pr), radiation parameter (N), magnetic field parameter (M), heat source parameter (Q), Schmidt number (Sc), suction parameter (f_w) and Eckert number (Ec) are confronted. The effects of these parameters on the velocity, temperature and concentration profiles are investigated.

Key Words: MHD, Forced Convection, Stretching sheet, Heat Generation, Radiation.

I. Introduction

Out of two types of convective heat and mass transfer, forced convection is the one where the velocity of the flow dominates over the other parameters. Some kind of external forces are employed here. The cooling system in a car engine is an example of forced convection. Thermal radiation effects may play an important role in controlling heat transfer in industry where the quality of the final product depends on the heat controlling factors to some extent. High temperature plasmas, cooling of nuclear reactors, liquid metal fluids, and power generation systems are some important applications of radiative heat transfer from a vertical wall to conductive gray fluids. Thermal radiation effect on forced and free convection have been studied in recent years extensively, as the magnetohydrodynamic [MHD] flow and heat transfer problems have become more important in many engineering and industrial applications. Hossain and Takhar [1] studied the radiation effects using the Rosseland diffusion approximation [2] (Seigel and Howell, 1972) that leads to non similar boundary layer equation governing the mixed convection flow of an optically dense viscous incompressible fluid past heated vertical plate with a free uniform velocity and surface temperature. Shateyi *et al*. [3] studied the thermal radiation and buoyancy effects on heat and mass transfer over a semi-infinite stretching surface with suction and blowing. Ali *et al*. [4] studied the radiation effect on natural convection flow over a vertical surface in a gray gas. Following Ali *et al*. Mansour [5] studied the interaction of mixed convection with thermal radiation in laminar boundary layer flow over a horizontal, continuous moving sheet with suction / injection. Elbashbeshy *et al*. [6] studied the determination of the effect of radiation on forced convection flow of a micropolar fluid over a horizontal plate. Aydin *et al*. [7] investigated the mixed convection heat transfer about a permeable vertical plate in the presence of magneto and thermal radiation effects. Cess [8] studied to determine the influence of radiation heat transfer upon the forced convection Nusselt number.

Samad and Rahman [9] investigated thermal radiation interaction with unsteady MHD flow past a vertical porous plate immersed in a porous medium. Samad and Karim [10] studied thermal radiation interaction with unsteady MHD free convection flow through a vertical flat plate with time dependent suction in the presence of magnetic field. As in the case of stretching sheets, Chen [11] studied laminar mixed convection adjacent to vertical continuously stretching sheet. Chiam [12] investigated magnetohydrodynamic heat transfer over non-isothermal stretching sheet. Pop *et al*. [13] studied radiation effect on the flow near the stagnation point of a stretching sheet. Abo-eldahab [14] studied flow and heat transfer in a micropolar fluid past a stretching surface embedded in a non-Darcian porous medium with uniform free stream. Samad *et al*. [15] investigated magnetohydrodynamic heat and mass transfer forced convection flow along a stretching sheet with heat generation/ absorption. T. S. Khaleque and Samad [16] studied the effects of radiation, heat generation and viscous dissipation on MHD free convection flow along a stretching sheet. In the present study thermal radiation interaction on MHD forced convection flow in the presence of a uniform magnetic field over a vertical stretching sheet with heat generation and viscous dissipation has been investigated.

II. Mathematical Formulation

We consider a steady two-dimensional magnetohydrodynamic heat and mass transfer flow of a viscous

incompressible fluid along a vertical stretching sheet with constant heat generation/absorption with radiation.

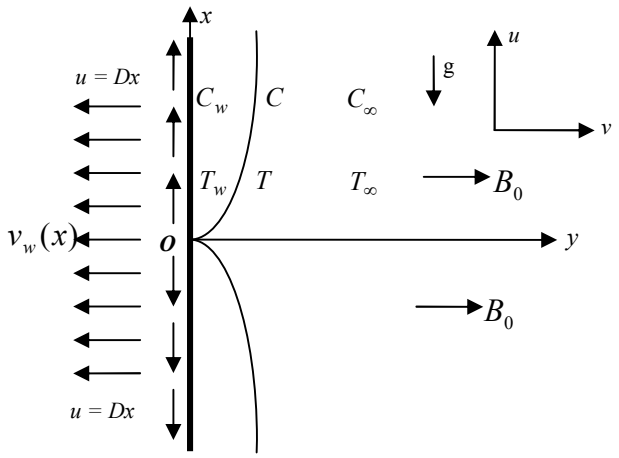

Fig.1: Flow configuration and Coordinate system.

We take the x-axis along the sheet and y-axis perpendicular to it. Two equal and opposite forces are introduced along the x-axis so that the sheet is stretched keeping the origin fixed. A uniform magnetic field of strength B_0 is imposed along the y-axis. A radiation depending on temperature is applied on the stretching sheet.

The governing equations representing the proposed flow field are:

Continuity Equation:

$$\frac{\partial u}{\partial x}+\frac{\partial v}{\partial y}=0 \tag{1}$$

Momentum Equation:

$$u\frac{\partial u}{\partial x}+v\frac{\partial u}{\partial y}=\nu\frac{\partial^2 u}{\partial y^2}+sg\beta(T-T_\infty)-\frac{\sigma B_0^2}{\rho}u \tag{2}$$

Energy Equation:

$$u\frac{\partial T}{\partial x}+v\frac{\partial T}{\partial y}=\frac{\kappa}{\rho C_p}\frac{\partial^2 T}{\partial y^2}+\frac{\nu}{C_p}\left(\frac{\partial u}{\partial y}\right)^2 +\frac{Q_0}{\rho C_p}(T-T_\infty)-\frac{1}{\rho C_p}\frac{\partial q_r}{\partial y} \tag{3}$$

Concentration Equation:

$$u\frac{\partial C}{\partial x}+v\frac{\partial C}{\partial y}=D_m\frac{\partial^2 C}{\partial y^2} \tag{4}$$

We take $s = 0$ to vanish the second term of the right hand side of (2) for the forced convection. After using the Rosseland approximation and applying the Taylor series expansion the energy equation (3) takes the form,

$$u\frac{\partial T}{\partial x}+v\frac{\partial T}{\partial y}=\frac{\kappa}{\rho C_p}\frac{\partial^2 T}{\partial y^2}+\frac{\nu}{C_p}\left(\frac{\partial u}{\partial y}\right)^2 +\frac{Q_0}{\rho C_p}(T-T_\infty)+\frac{16}{3}\frac{\sigma_1 T_\infty^3}{\rho C_p k_1}\frac{\partial^2 T}{\partial y^2} \tag{5}$$

Here, the second term in the right hand side refers to the viscous dissipation term.

The boundary conditions as a whole are

$$\left.\begin{aligned} &u=Dx,\quad v=v_w,\quad T=T_w,\quad C=C_w \text{ at } y=0,\\ &u=0,\quad T=T_\infty,\quad C=C_\infty \qquad\qquad \text{as } y\to\infty \end{aligned}\right\} \tag{6}$$

The following similarity variables are introduced to obtain a similarity solution corresponding to the above problem.

$$\eta=y\sqrt{\frac{D}{\nu}} \tag{7}$$

$$\psi=\sqrt{D\nu}\,xf(\eta) \tag{8}$$

$$\theta(\eta)=\frac{T-T_\infty}{T_w-T_\infty} \tag{9}$$

$$\phi(\eta)=\frac{C-C_\infty}{C_w-C_\infty} \tag{10}$$

Here ψ is the stream function, η is the dimensionless distance normal to the sheet, f is the dimensionless stream function, θ is the dimensionless fluid temperature and ϕ is the dimensionless concentration.

Since $u=\frac{\partial\psi}{\partial y}$ and $v=-\frac{\partial\psi}{\partial x}$ we have the velocity components from equation (14) given by

$$\left.\begin{aligned} u&=Dxf'(\eta)\\ v&=-\sqrt{D\nu}\,f(\eta) \end{aligned}\right\} \tag{11}$$

Here prime denotes the derivatives with respect to η.

Now substituting the similarity variables from equations (7) to (10) into the equations (2), (5) and (4) we have the system as,

$$f'''+ff''-(f')^2-Mf'=0 \tag{12}$$

$$\theta''+\frac{3N\,\mathrm{Pr}}{3N+4}f\theta'+\frac{3N\,\mathrm{Pr}\,Q}{3N+4}\theta +\frac{3N\,\mathrm{Pr}\,Ec}{3N+4}(f'')^2=0 \tag{13}$$

$$\phi''+Scf\phi'=0 \tag{14}$$

The transformed boundary conditions are:

$$\left.\begin{aligned} f' = 1, \quad f = f_w, \quad \theta = 1, \quad \phi = 1 \quad \text{at } \eta = 0 \\ f' = 0, \quad \theta = 0, \quad \phi = 0 \qquad \text{as } \eta \to \infty \end{aligned}\right\} \quad (15)$$

Here, $M = \dfrac{\sigma B_0^2}{\rho D}$ is the magnetic field parameter, $\Pr = \dfrac{\mu C_p}{\kappa}$ is the Prandtl number, $Q = \dfrac{Q_0}{\rho C_p D}$ is the heat source/ sink parameter, $N = \dfrac{\kappa k_1}{4\sigma_1 T_\infty^3}$ is the radiation parameter and, $f_w = -\dfrac{v_w}{\sqrt{D\nu}}$ is the suction parameter.

III. Numerical Computations

The nonlinear ordinary differential equations (18), (19) and (20) under the boundary conditions (21) are solved numerically for various values of the parameters occurring in the problem. Here we use the standard initial-value solver shooting method namely Nachtsheim-Swigert (1965) [17] shooting iteration technique (guessing the missing value) together with the sixth order Runge-Kutta-Butcher initial value solver.

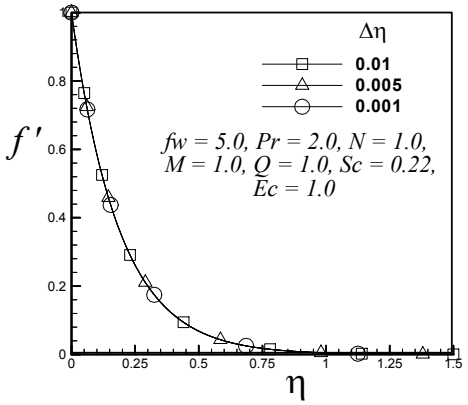

Fig. 2(a). Velocity profiles for various step sizes.

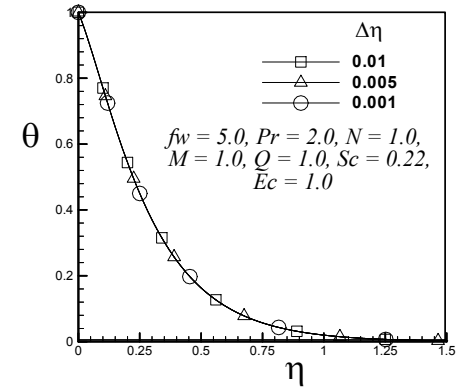

Fig. 2(b). Temperature profiles for various step sizes.

A step size of $\Delta\eta = 0.001$ has been used together with accuracy of 10^{-6} in all the cases. The value of $\eta_{\max}$ was selected in accordance with the values of each group of parameters Pr, f_w, M, Q, N and Ec to satisfy the accuracy requirement. The code verifying graphs for different step sizes are shown in the **Fig. 2(a)** and **Fig. 2(b)**. Here, we see that for step sizes, $\Delta\eta = 0.01, 0.005, 0.001$ the velocity and the temperature profiles are in fine agreement among them.

IV. Results and Discussion

We use the dimensionless velocity, temperature, and concentration profiles to present the results obtained in the numerical computations. Numerical computations have been carried out for various values of the parameters entering into the problem in compliance with the different physical conditions. These parameters are, the Prandtl number (Pr), suction parameter (f_w), magnetic field parameter (M), radiation parameter (N), Schmidt number (Sc), heat source parameter (Q) and Eckert number (Ec).

Significant effect of Prandtl number variation is observed in the temperature field shown in the **Fig. 3**. The temperature profiles increase up to a value of about $\eta = 0.15$ and then it start to decrease with the increase of the Prandtl number. The thermal boundary layer decreases with the increase of the Prandtl number. We see that for air that is, for Pr = 0.71 the thermal boundary layer is thicker than that for the other values of Pr. With the increase of the Prandtl number the thermal boundary layer thickness start to decrease. For Pr = 7.0 the temperature rises the most and then rapidly decrease. The result is in good agreement with that given by Samad *et al*. [15].

Fig. 4 shows the effect of radiation parameter on the velocity, temperature and concentration profiles. The velocity profiles in the **Fig. 4 (a)** do not show any significant effect.

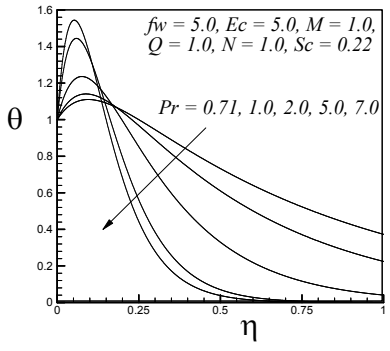

Fig. 3. Temperature profiles for various values of Prandtl numbers.

This is because of the fact that in the forced convection the velocity is relatively large Therefore, no significant effects in the velocity profiles are observed. The momentum boundary layer thickness does not change due to variations in the radiation parameters. The temperature profiles have sharp effects as shown in the **Fig. 4(b)**. The temperature profiles cross each other near about $\eta = 0.12$. The temperature at first rises and then decreases down. The thermal boundary layer thickness also changes due to the change in the radiation parameter. For $N = 0.10$ the thermal boundary layer thickness is very high. As the radiation parameter value increases the thermal boundary layer thickness also decreases.

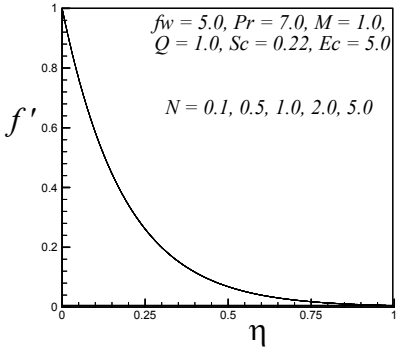

Fig. 4(a). Velocity profiles for various values of radiation parameter.

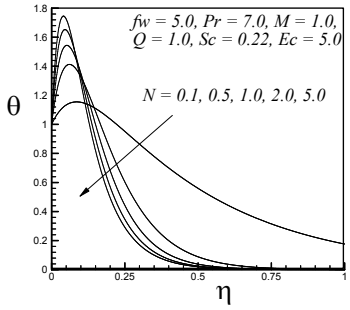

Fig. 4(b). Temperature profiles for various values of radiation parameter.

In the **Fig. 5** it is shown that all the dimensionless velocity, temperature, and concentration profiles have effects for the variation in the magnetic field parameter *M*. The velocity profiles are shown in the **Fig. 5(a)**. We see that the velocity profiles decrease with the increase in the magnetic field parameter values. This happens due to the retarding effect of the magnetic field in the flow field. The momentum boundary layer thickness decreases with the increase of the magnetic field parameter values. This indicates we can effectively use the magnetic field to control the boundary layer. The temperature profiles are shown in the **Fig. 5(b)**.

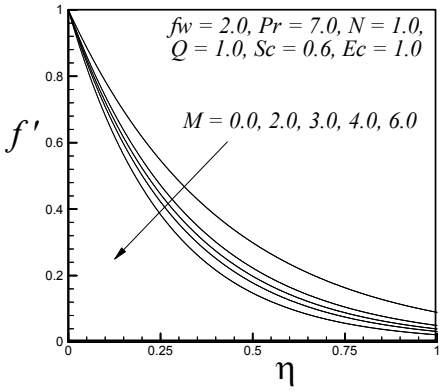

Fig. 5(a). Velocity profiles for values of magnetic field parameter.

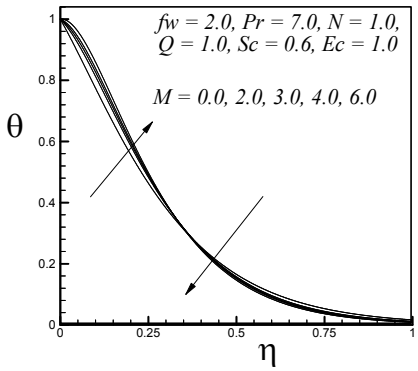

Fig. 5(b). Temperature profiles for values of magnetic field parameter.

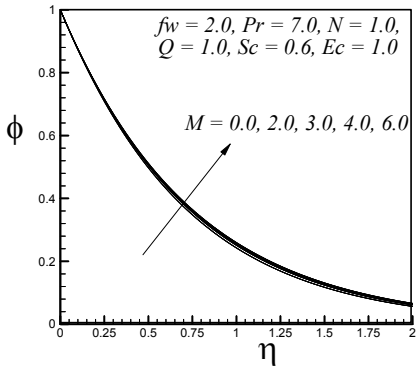

Fig. 5(c). Concentration profiles for various values of magnetic field parameter.

The temperature profiles at first mark an increase and then decrease with the increase of the magnetic field parameter. The thermal boundary layer thickness also changes a small amount due to the increase in the magnetic field parameter. The concentration profiles are shown in **Fig. 5(c)**. They show a slight increase with the increase of the magnetic field parameter. This occurs because the magnetic effect on the fluid particles increases the fluid concentrations. The results are analogous in Samad *et al*. [15]. A small difference is observed in the temperature profiles. This is

due to the changed values of the various parameters and the presence of additional parameters as radiation and viscous dissipation.

The concentration profiles show a sharp change for the change in the Schmidt number (*Sc*). This is shown in the **Fig. 6**. With the increase in the Schmidt number the concentration profiles mark a major decrease. The concentration boundary layer thickness also changes with the increase in the Schmidt number (Samad *et al*. [16]).

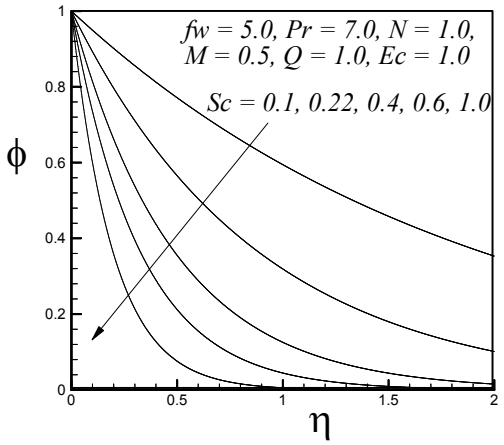

Fig. 6. Concentration profiles for various values of Schmidt number.

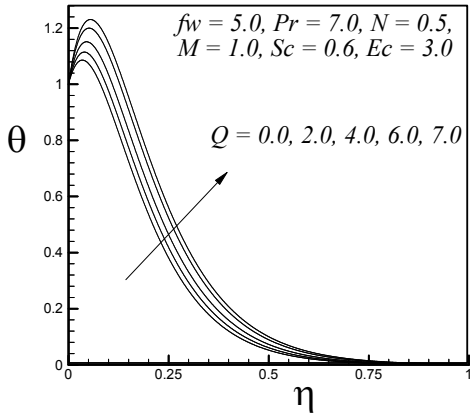

Fig. 7. Temperature profiles for values of heat source parameter.

The temperature profiles in the **Fig. 7** shows effects with the change in the heat source parameter. The temperature increases at first as the heat source parameter increases. Then it decreases gradually. This is evident as because the increase in the heat source parameter will obviously increase the temperature. The thermal boundary layer thickness changes significantly in Samad *et al*. [15], but in the present work this change is insignificant owing to the presence of viscous dissipation in the flow field.

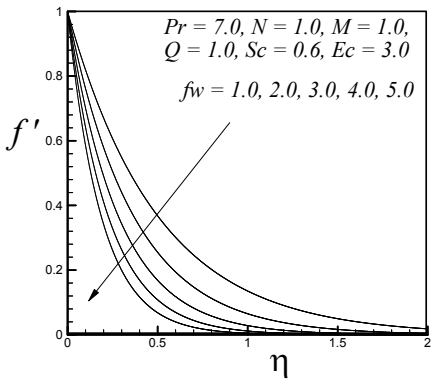

Fig. 8(a). Velocity profiles for various values of suction parameter.

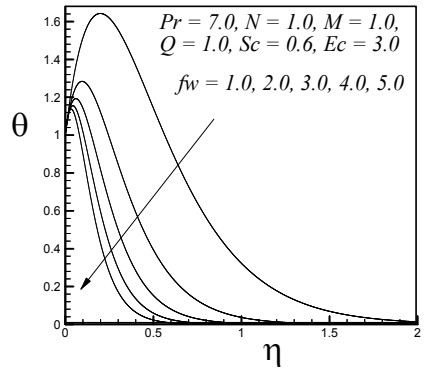

Fig. 8(b). Temperature profiles for various values of suction parameter.

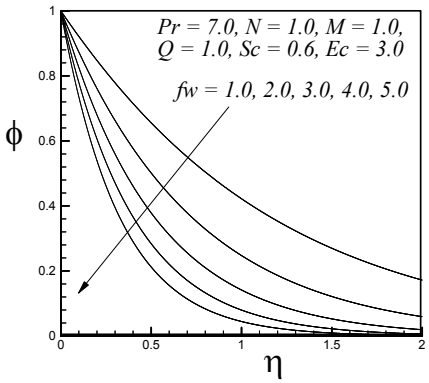

Fig. 8(c). Concentration profiles for various values of suction parameter.

In the **Fig. 8** the effect of suction parameter is shown. Here in this case, the dimensionless velocity profiles in the **Fig. 8(a)** shows a decrease with the increase in the suction parameter. This is because the increase in the suction parameter contributes more to remove the boundary layer materials from the flow field. Also for this reason the boundary layer thickness decreases with the increase of the suction parameter.

The temperature profiles are shown in the **Fig. 8(b)**. Here we see that the temperature rises rapidly when suction parameter has a smaller value, that is, 1.0. As the suction

parameter value increases the temperature starts to decrease evidently. The thermal boundary layer decreases a large amount with the increase of the suction parameter. The concentration profiles are exhibited in the **Fig. 8(c)**. As evident they also show a sharp decrease with the increase of the suction parameters. The results show a resemblance with Samad *et al* [15].

Finally the variation of Eckert number is shown in the **Fig. 4.9**. The temperature profiles show a sharp increase with the increase of the Eckert number. This happens due to the buoyancy effects on the flow field. The thermal boundary layer thickness changes a small amount.

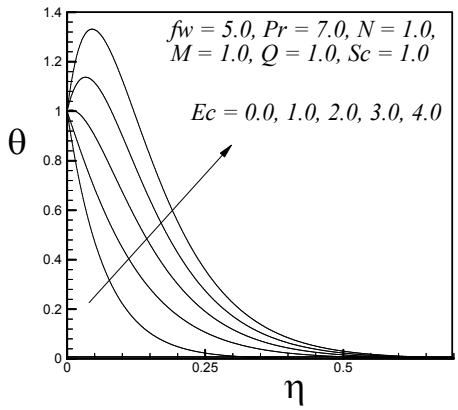

Fig. 9. Temperature profiles for various values of Eckert number.

V. Skin-Friction Coefficient, Nusselt Number and Sherwood Number

The skin friction coefficient (C_f), local Nusselt number (Nu_x) and the local Sherwood numbers (Sh) are significant in the engineering field. These parameters refer to the wall shear stress, local wall heat transfer rate and wall mass transfer rate respectively. It is observed that the skin-friction coefficient, Nusselt number, and Sherwood number are proportional to $f''(0), -\theta'(0),$ and $-\phi'(0)$ respectively. Tables comprising of the proportional values of C_f, Nu_x, and Sh corresponding to the previous graphs are shown in the following tables. The numerical values are in excellent agreement compared to Samad *et al*. (2010)[15]. The local heat transfer rate i. e., Nu_x shows some change caused by the additional parameters introduced in the energy equation (3).

Table. 1(a). Values of C_f compared to published results for Pr.

Pr	Samad *et al*. (2010)	Present
0.71	-2.7320508	-2.73204947
1.0	-2.7320508	-2.73204947
2.0	-2.7320508	-2.73204947
5.0	-2.7320508	-2.73204947
7.0	-2.7320508	-2.73204947

Table. 1(b). Values of *Sh* compared to published results for Pr.

Pr	Samad *et al*. (2010)	Present
0.71	0.5087632	0.5087415580
1.0	0.5087632	0.5087415580
2.0	0.5087632	0.5087415580
5.0	0.5087632	0.5087415580
7.0	0.5087632	0.5087415580

Table. 1(c). Values of Nu_x compared to published results for Pr.

Pr	Samad *et al*. (2010)	Present
0.71	0.8286300	-1.54985034
1.0	1.6537599	-2.46155882
2.0	3.7980496	-3.96453762
5.0	5.8496183	-5.67043161
7.0	13.92240342	-12.6296883

Table. 2(a). Values of C_f compared to published results for *M*.

M	Samad *et al*. (2010)	Present
0.0	-2.4141902	-2.41419435
0.5	-2.5811381	-2.58113670
1.0	-2.7320508	-2.73204947
1.5	-2.8708287	-2.87083077
2.0	-3.0000000	-3.00000000

Table. 2(b). Values of *Sh* compared to published results for *M*.

M	Samad *et al*. (2010)	Present
0.0	0.5159002	0.515867054
0.5	0.5119731	0.511951745
1.0	0.5087632	0.508741558
1.5	0.5060452	0.506033778
2.0	0.5037042	0.503655314

Table. 2(c). Values of Nu_x compared to published results for *M*.

M	Samad *et al*. (2010)	Present
0.0	0.9171173	-0.96421212
0.5	0.8731519	-1.30510569
1.0	0.8286300	-1.54985034
1.5	0.7814263	-1.74652600
2.0	0.7297744	-1.93507540

Table. 3(a). Values of C_f compared to published results for f_w.

f_w	Samad *et al*. (2010)	Present
1.0	-1.8228756	-1.82287526
2.0	-2.5811381	-2.58113670
3.0	-3.4364888	-3.43648672
4.0	-4.3452024	-4.34520149
5.0	-5.2838748	-5.28387403

Table. 3(b). Values of *Sh* compared to published results for f_w.

f_w	Samad *et al*. (2010)	Present
1.0	0.3231120	0.323111653
2.0	0.5119731	0.511972487
3.0	0.7139407	0.713940501
4.0	0.9227363	0.922734082
5.0	1.1352630	1.135262130

Table. 3(c). Values of Nu_x compared to published results for . f_w.

f_w	Samad *et al*. (2010)	Present
1.0	6.8222028	-11.7348986
2.0	13.9267745	-11.3599815
3.0	20.9544151	-12.5722971
4.0	27.9670449	-14.4075994
5.0	34.9741637	-16.5606899

Table. 4(a). Values of C_f compared to published results for *Sc*.

Sc	Samad *et al*. (2010)	Present
0.10	-5.2838768	-5.28387737
0.22	-5.2838748	-5.28387403
0.40	-5.2838755	-5.28387499
0.60	-5.2838781	-5.28387165
1.0	-5.2838858	-5.28387117

Table. 4(b). Values of *Sh* compared to published results for *Sc*.

Sc	Samad *et al*. (2010)	Present
0.10	0.5182383	0.518236339
0.22	1.1352630	1.135262130
0.40	2.0554354	2.055433030
0.60	3.0726143	3.071894170
1.0	5.0960873	5.096056940

Table. 4(c). Values of Nu_x compared to published results for *Sc*.

Sc	Samad *et al*. (2010)	Present
0.10	3.4260552	-1.84671140
0.22	3.4260552	-1.84670484
0.40	3.4260553	-1.84610283
0.60	3.4271237	-1.84387004
1.0	3.4287257	-1.84372818

Table. 5(a): Values of C_f compared to published results for *Q*.

Q	Samad *et al*. (2010)	Present
0.0	-5.2838748	-5.28387403
4.0	-5.2838748	-5.28387403
6.0	-5.2838748	-5.28387403
6.5	-5.2838748	-5.28387403
7.0	-5.2838748	-5.28387403

Table. 5(b): Values of *Sh* compared to published results for *Q*.

Q	Samad *et al*. (2010)	Present
0.0	1.1352630	1.13526213
4.0	1.1352630	1.13526213
6.0	1.1352630	1.13526213
6.5	1.1352630	1.13526213
7.0	1.1352630	1.13526213

Table. 5(c): Values of Nu_x compared to published results for *Q*.

Q	Samad *et al*. (2010)	Present
0.0	4.8956569	-2.19169402
4.0	4.1545981	-3.88645148
6.0	3.3577185	-4.97492886
6.5	2.9874869	-7.65185165
7.0	-0.712810	-1.23525465

Table. 6: C_f, Nu_x and *Sh* for different values of *N*.

N	C_f	Nu_x	*Sh*
0.10	-5.372278	-4.36887	1.1348044
0.50	-5.372278	-16.4397	1.1348044
1.0	-5.372278	-25.7225	1.1348044
2.0	-5.372278	-35.9357	1.1348044
5.0	-5.372278	-47.2249	1.1348044

Table. 7: C_f, Nu_x **and** ***Sh*** **for different values of** ***Ec*****.**

Ec	C_f	Nu_x	*Sh*
0.0	-5.372275	14.947803	5.096110
1.0	-5.372275	6.8137335	5.096110
2.0	-5.372275	-1.320334	5.096110
3.0	-5.372275	-9.454403	5.096110
4.0	-5.372275	-17.58847	5.096110

VI. Conclusion

The problem has dealt with the two dimensional heat and mass transfer forced convection flow of an MHD fluid along a vertical stretching sheet in the presence of magnetic field with heat generation, radiation and viscous dissipation.

From the results obtained in the present analysis and comparing with the results by Samad *et al.* [15] the following conclusions can be made:

1. In the forced convection the velocity being large, the Prandtl number has no effective dominance over velocity and concentration. Nevertheless on the temperature it has a significant effect. With viscous dissipation taken into consideration, local heat transfer rate decreases with the increase of the Prandtl number.
2. The radiation parameter has a large effect on the temperature profiles, and hence can be used effectively to control the temperature of the flow field.
3. The magnetic parameter has significant effect on the velocity, temperature and concentration profiles. The local skin-friction coefficient, heat transfer rate and mass transfer rate decrease with the increase of the magnetic parameter. So, magnetic field can effectively be used to control the flow field.
4. As apparent the temperature increases within the boundary layer with the increase of the heat source parameter.
5. For the increase of the suction parameter the velocity, temperature and concentration significantly decrease and as a consequence making it one of the most essential parameter in the boundary layer control theory.
6. The Schmidt number has large effects on the concentration profiles dominating the mass transfer rate of the flow.
7. The effect of Eckert number is clearly visible on the flow pattern. With viscous dissipation in effect the temperature rises in the vicinity of the wall.

---

1. Hossain, M. A., H. S. Takhar, 1996. Radiation Effect on Mixed Convection along a Vertical Plate with Uniform Surface Temperature. Heat and Mass Trans. **31(4)**, 243-248.
2. Seigel, R., J. R. Howell, 1972. Thermal Radiation Heat Transfer. McGraw-Hill, New York.
3. Shateyi, S., M. Petersen, 2008. Thermal Radiation and Buoyancy Effects on Heat and Mass Transfer over a Semi-Infinite Stretching Surface with Suction and Blowing. J. Appl. Math. **2008** (2008), 12.
4. Ali, M. M., T. S. Chen, and B. F. Armaly, 1984. Natural Convection Radiation Interaction In Boundary Layer Flow over Horizontal Surfaces. AIAA Journal, **22(12)**, 797-803.
5. Mansour, M. A, 1990. Radiative and Free Convection Effects on the Oscillatory Flow past a Vertical Plate. Astrophysics Space Sci. **166**, 269-275.
6. Elbashbeshy, E. M. A., M. A. A. Bazid, 2000. Effect of Radiation on Forced Convection Flow of a Micropolar Fluid over a Horizontal Plate. Can. J. Phys. **78**, 907-913.
7. Aydin, O., A. Kaya, 2008. Radiation Effect On MHD Mixed Convection Flow About A Permeable Vertical Plate. Heat Mass Trans. **45**, 239-246.
8. Cess, R. D., 1966. The Effect of Radiation upon Forced Convection Heat Transfer, Appl. Sci. Res. Sec A. **10**, 1269-1277.
9. Samad, M. A., M. M. Rahman, 2006. Thermal Radiation Interaction with Unsteady MHD Flow past a Vertical Porous Medium. J. Nav. Arch. Mar. Eng. **3**, 7-14.
10. Samad, M. A., M. E. Karim, 2009. Thermal Radiation Interaction with Unsteady MHD Flow past a Vertical Flat Plate with Time Dependent Suction. Dhaka Univ. J. Sci. **57(1)**, 113-118.
11. Chen, C. H., 1998. Laminar Mixed Convection Adjacent to Vertical, Continuously Stretching Sheet. Heat and Mass Tran. **33**, 471-476.
12. Chiam, T. C., 1997. Magnetohydrodynamic Heat Transfer over a Non-Isothermal Stretching Sheet. Acta Mechanica. **122**, 169-179.
13. Pop. S. R., T. Grosan, I. Pop, 2004. Radiation Effect on the Flow near the Stagnation Point of a Stretching Sheet. The Chnische Mechanik, **25**, 100-106.
14. Abo-Eldahab, E. M., 2005. Flow And Heat Transfer in a Micropolar Fluid past a Stretching Surface Embedded in a Non-Darcian Porous Medium with Uniform Free Stream. Appl. Math. Comp. **162**, 881-889.
15. Samad, M. A., M. Mohebujjaman, M. Mustak Mia, M. A. Rahman, 2010. Magnetohydrodynamic heat and Mass Transfer Forced Convection Flow along a Stretching Sheet with Heat Generaion/ Absorption. Dhaka Univ. J. Sci. **58(1)**, 91-96.
16. Khaleque, T. S., M. A. Samad, 2010. Effects of Radiation, Heat Generation and Viscous Dissipation on MHD Free Convection Flow along a Stretching Sheet. Res. J. Appl. Sci. Eng. Technol., **1(3)**, 98-106.
17. Nachtsheim, P. R., P. Swigert, 1965. Satisfaction of the Asymptotic Boundary Conditions in Numerical Solution of the System of Non-Linear Equations of Boundary Layer Type. NASA TND-3004.